

## Supplemental Figure Legend:

### Figure S1. Kaplan–Meier plot of breast cancer patient survival when stratified according to LGR5–8 mRNA expression.

A. LGR5: OS, overall Survival ( $n_{\text{high}} = 557, n_{\text{low}} = 560$ ); DMFS, Distant Metastasis Free Survival ( $n_{\text{high}} = 793, n_{\text{low}} = 816$ ); RFS, Relapse Free Survival ( $n_{\text{high}} = 1741, n_{\text{low}} = 1813$ ); PPS, post progression survival ( $n_{\text{high}} = 172, n_{\text{low}} = 179$ ).

B. LGR6: OS ( $n_{\text{high}} = 260, n_{\text{low}} = 262$ ); DMFS ( $n_{\text{high}} = 331, n_{\text{low}} = 333$ ); RFS ( $n_{\text{high}} = 830, n_{\text{low}} = 830$ ), PPS ( $n_{\text{high}} = 70, n_{\text{low}} = 70$ ).

C. LGR7: OS ( $n_{\text{high}} = 260, n_{\text{low}} = 262$ ); DMFS ( $n_{\text{high}} = 331, n_{\text{low}} = 333$ ); RFS ( $n_{\text{high}} = 806, n_{\text{low}} = 854$ ); PPS( $n_{\text{high}} = 70, n_{\text{low}} = 70$ ).

D. LGR8: OS ( $n_{\text{high}} = 255, n_{\text{low}} = 267$ ); DMFS ( $n_{\text{high}} = 324, n_{\text{low}} = 340$ ); RFS( $n_{\text{high}} = 815, n_{\text{low}} = 845$ ); PPS( $n_{\text{high}} = 69, n_{\text{low}} = 71$ ). OS: Overall Survival; RFS: Relapse Free Survival; DMFS: Distant Metastasis Free Survival, and PPS: Post-Progression Survival.

### Figure S2. LGR4 expression was correlated with the invasive ability of different cell lines.

A. Heatmap of LGR family mRNA expression in 45 different immortalized normal breast or breast cancer cell lines. Data (GEO Accession Number GSE10890) values in  $\log_2$  of expression signal were sorted and analyzed. Scale bar: red indicates high expression and green represents low mRNA expression.

B-C. Invasive abilities of 6 breast cancer cell lines identified by Boyden chamber invasion assay in vitro. The invasive cells were stained followed by photography (B), and quantitation (C). As shown in the blue by red arrow, invasive potential weak and strong were divided by the average of different invasive cell number. Experiment was independently repeated three times and graphs show the means  $\pm$  S.D. Scale bars, 100  $\mu\text{m}$ .

D. *LGR4* expression in 6 human breast cancer cell lines of differing invasiveness, as determined by qPCR. Experiment was repeated three times.

**Figure S3. *Lgr4* heterozygosity delays mammary tumor onset and progression in MMTV-PyMT transgenic mice.**

A. *Lgr4* mRNA levels in mammary tumors from PyMT-*Lgr4*<sup>+/+</sup>, -*Lgr4*<sup>+/-</sup> and -*Lgr4*<sup>-/-</sup> mice at 12 weeks, as identified by qPCR.

B-C. *Lgr4* heterozygosity delayed tumor formation in MMTV-PyMT transgenic mice. Representative images of H & E stained sections from mammary glands of indicated mice (C). Classification of mammary gland lesions in 9-, 13- and 15-week-old MMTV-PyMT mice with indicated *Lgr4* genotype (B). Scale bars, 500  $\mu$ m. IDC: Invasive ductal carcinoma; DCIS: Ductal carcinoma in situ; ADH: Atypical ductal hyperplasia; PL: Proliferative lesion without atypia; N: Normal.

D. PCNA staining of tumors from 9-, 13- and 15-week-old MMTV-PyMT mice of indicated *Lgr4* genotype. Scale bars, 200  $\mu$ m.

**Figure S4. *Lgr4* regulates the breast tumor onset and metastasis to the lungs in MMTV-PyMT mice and transfection efficiency testing in different BrCa cell migration and invasion assay.**

A. Whole mount of indicated mice at 3.5 weeks of age.

B. Kaplan–Meier plot showing palpable tumor-free mice until 120 days of age. PyMT-*Lgr4*<sup>+/+</sup> ( $n = 11$ ) and PyMT-*Lgr4*<sup>+/-</sup> ( $n = 13$ ). Log-rank test was used to determine  $P$  values.

C. *Lgr4* heterozygosity reduced the number of tumors per mouse in MMTV-PyMT mice. Error bars are mean  $\pm$  S.D. \* $P < 0.05$ .  $n = 7$  per group.

D. The volume of primary tumors until 12 weeks between PyMT-*Lgr4*<sup>+/+</sup> and PyMT-*Lgr4*<sup>+/-</sup> mice. Error bars are mean  $\pm$  S.D. \*\* $P < 0.01$ ; \*\*\* $P < 0.001$ .  $n = 7$  per group.

E. H & E staining of lung sections from 15-week-old mice of indicated genotype. Scale bars, 500  $\mu$ m.

F. Graph shows quantitation of metastatic foci in lungs of MMTV-PyMT *Lgr4*<sup>+/+</sup> and MMTV-PyMT *Lgr4*<sup>+/-</sup> mice.  $n = 6$  mice per group. Error bars are mean  $\pm$  S.D. \*\*\* $P < 0.001$ .

G-J. *LGR4* knockdown or overexpression efficiency related to Fig. 4A-4D, respectively,

tested by qPCR analysis. Experiment was independently repeated three times and representative graphs show the means  $\pm$  S.D. \* $P < 0.05$ ; \*\* $P < 0.01$ ; \*\*\* $P < 0.001$ .

**Figure S5. LGR4 did not regulate cAMP-CREB signaling in breast cancer**

A. The adenosine 3',5'-cyclic monophosphate (cAMP) level was examined by ELISA in PyMT-*Lgr4* CKO and PyMT-*Lgr4*<sup>fl/fl</sup> tumors cells (n=3 mice for each group, experiments conducted in triplicate).

B. Active phosphoSer133-CREB in PyMT-*Lgr4* CKO mice tumors was examined using a specific anti-phospho-CREB antibody by Western blot analysis.

C. Treated with 50  $\mu$ M forskolin activated cAMP in MDA-MB-231 knockdown LGR4 cells. p-FAK was examined by Western blot analysis. Experiment was independently repeated three times.

**Supplemental Table 1: Primer sequences used in this study.**

<b>Target Gene for qRT-PCR</b>	<b>Forward primer 5' -&gt; 3'</b>	<b>Reverse primer 5' -&gt; 3'</b>
<b>Human <i>LGR4</i></b>	5'ACCTGGAGACCTTAGACTT G3'	5'CCACGAATGACTAGGGAAT G3'
<b>Human <i>Oct4</i></b>	5'CTGCAGAAGGAGCTAGAA CAGT3'	5'CTCGAAGCGACAGATGGTG 3'
<b>Human <i>Sox2</i></b>	5'TACAGCATGTCCTACTCGC AG3'	5'GAGGAAGAGGTAACCCACAG GG3'
<b>Human <i>Axin2</i></b>	5'TAGGTTCTGGCTATGTCTT TG3'	5'GTATCGTCTGCGGGTCTT3'
<b>Human <i>Snail1</i></b>	5'ATCGGAAGCCTAACTACAG C3'	5'TTTCCCACTGTCCTCATCTG 3'
<b>Human <i>Slug</i></b>	5'CGAACTGGACACACATAC AGTG3'	5'CTGAGGATCTCTGGTTGTG GT3'
<b>Human <i>Twist</i></b>	5' GCAAGATTCAGACCCTCA AG3'	5'AGTTATCCAGCTCCAGAGT C3'
<b>Human <i>N-cadherin</i></b>	5'GTGCCATTAGCCAAGGGA ATTCAGC3'	5'TGGCACGTCTTGACCTTGA A3'
<b>Human <i>E-cadherin</i></b>	5'TCCATTTCTTGGTCTACGC C3'	5'CACCTTCAGCCAACCTGTTT 3'
<b>Mouse <i>Lgr4</i></b>	5'AAGATAACAGCCCCCAAG AC3'	5'AGGCAGTGATGAACAAGAC G3'

**Supplemental Table 2: Antibody information in this study.**

<b>Antibody Target</b>	<b>Supplier</b>	<b>Catalog Number</b>	<b>Application</b>	<b>Dilution</b>
<b>Cofilin</b>	Cell Signaling Technologies (CST)	3312	immunoblot	1:1000
<b>phosphoCofilin</b>	CST	3313	immunoblot	1:1000
<b>Cyclin D1</b>	Abcam	ab134175	immunoblot	1:1000
<b>E-cadherin</b>	CST	3195	immunoblot	1:1000
<b>Vimentin</b>	CST	5741	immunoblot	1:1000
<b>ZEB1</b>	CST	3399	immunoblot	1:1000
<b>phosphoERK</b>	CST	4377	immunoblot	1:1000
<b>ERK</b>	CST	9102	immunoblot	1:1000
<b>phosphoFAK</b>	CST	3283	immunoblot	1:1000
<b>FAK</b>	Santa Cruz	sc-557	immunoblot	1:200
<b>P-CREB</b>	CST	9198	immunoblot	1:1000
<b>CREB</b>	CST	9197	immunoblot	1:1000
<b>GAPDH</b>	CST	5174	immunoblot	1:1000
<b>β-actin</b>	Sigma	A5441	immunoblot	1:1000
<b>phosphoSrc</b>	CST	2101	immunoblot	1:1000
<b>Src</b>	CST	2108	immunoblot	1:1000
<b>IRDye® 800CW Goat anti-Mouse IgG</b>	LI-COR	925-32210	immunoblot	1:10000
<b>IRDye® 800CW Goat anti-Rabbit IgG</b>	LI-COR	925-32211	immunoblot	1:10000
<b>Rhodamine Phalloidin</b>	Thermo-Molecular Probes™	R415	immunofluorescence	1:20
<b>Vinculin</b>	Santa curz	sc-55465	immunofluorescence	1:200
<b>PCNA</b>	Santa curz	sc-7907	immunohistochemical	1:200
<b>β-catenin</b>	CST	9562	immunohistochemical	1:200
<b>Cyclin D1</b>	Abcam	ab134175	immunohistochemical	1:200
<b>Human LGR4 antibody</b>	Dr. Qingyun (Jim) Liu		immunohistochemical	1:200
<b>Goat anti-Rat IgG Secondary Antibody</b>	Thermo Fisher	62-9520	immunohistochemical	1:1000

Figure S1

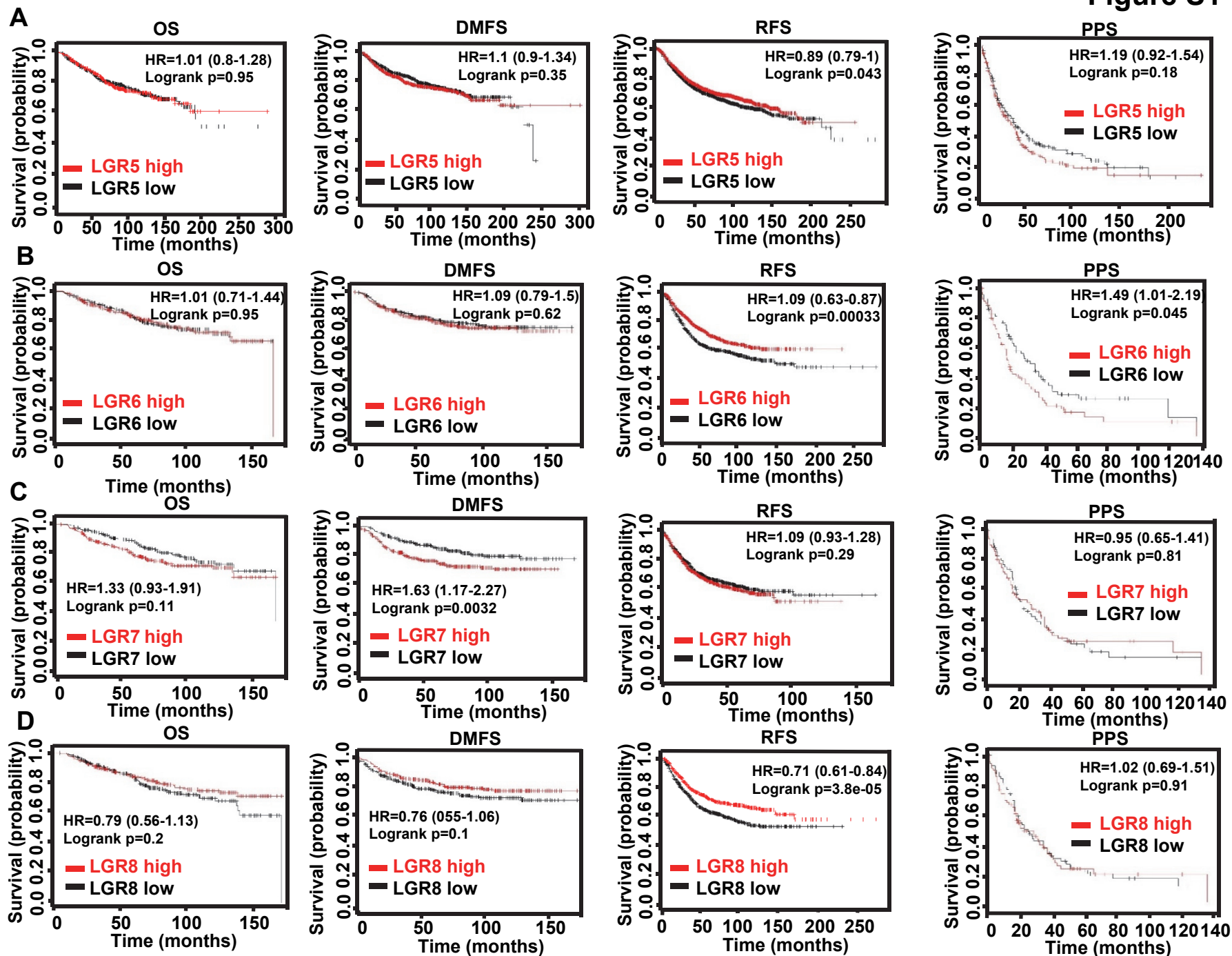


Figure S2

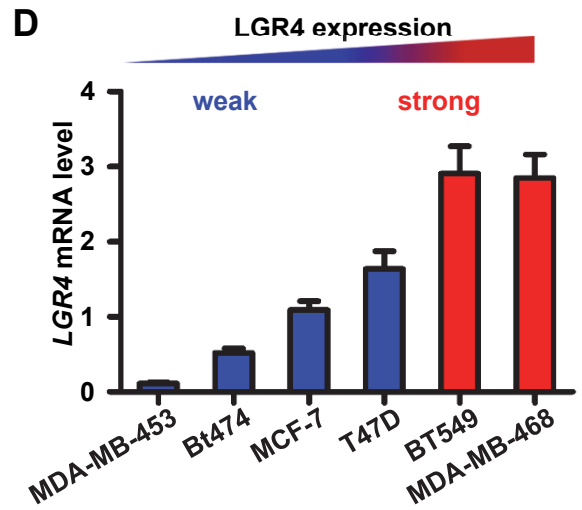
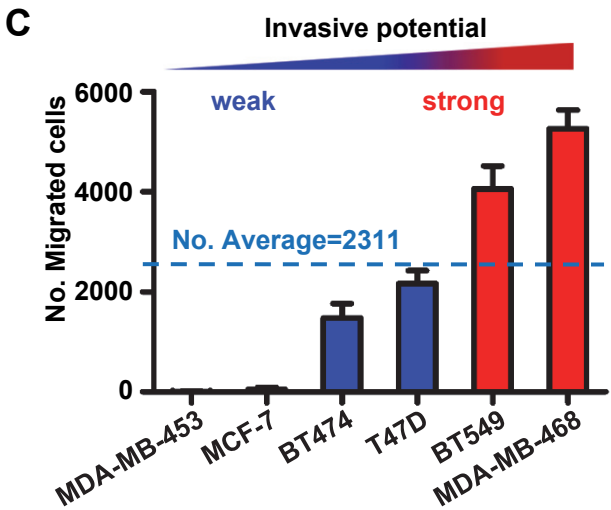
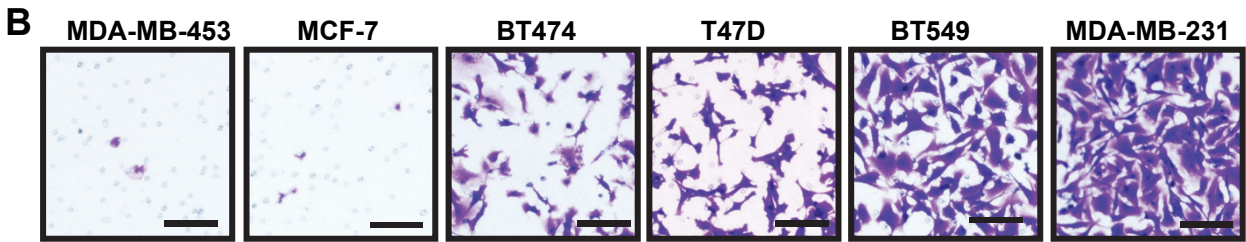
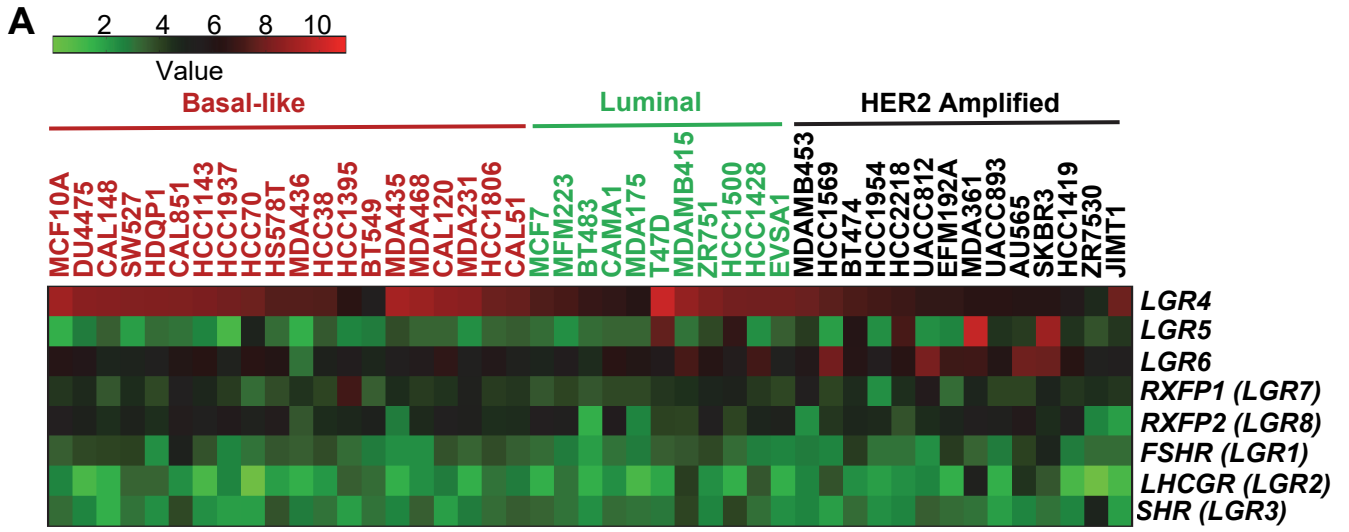
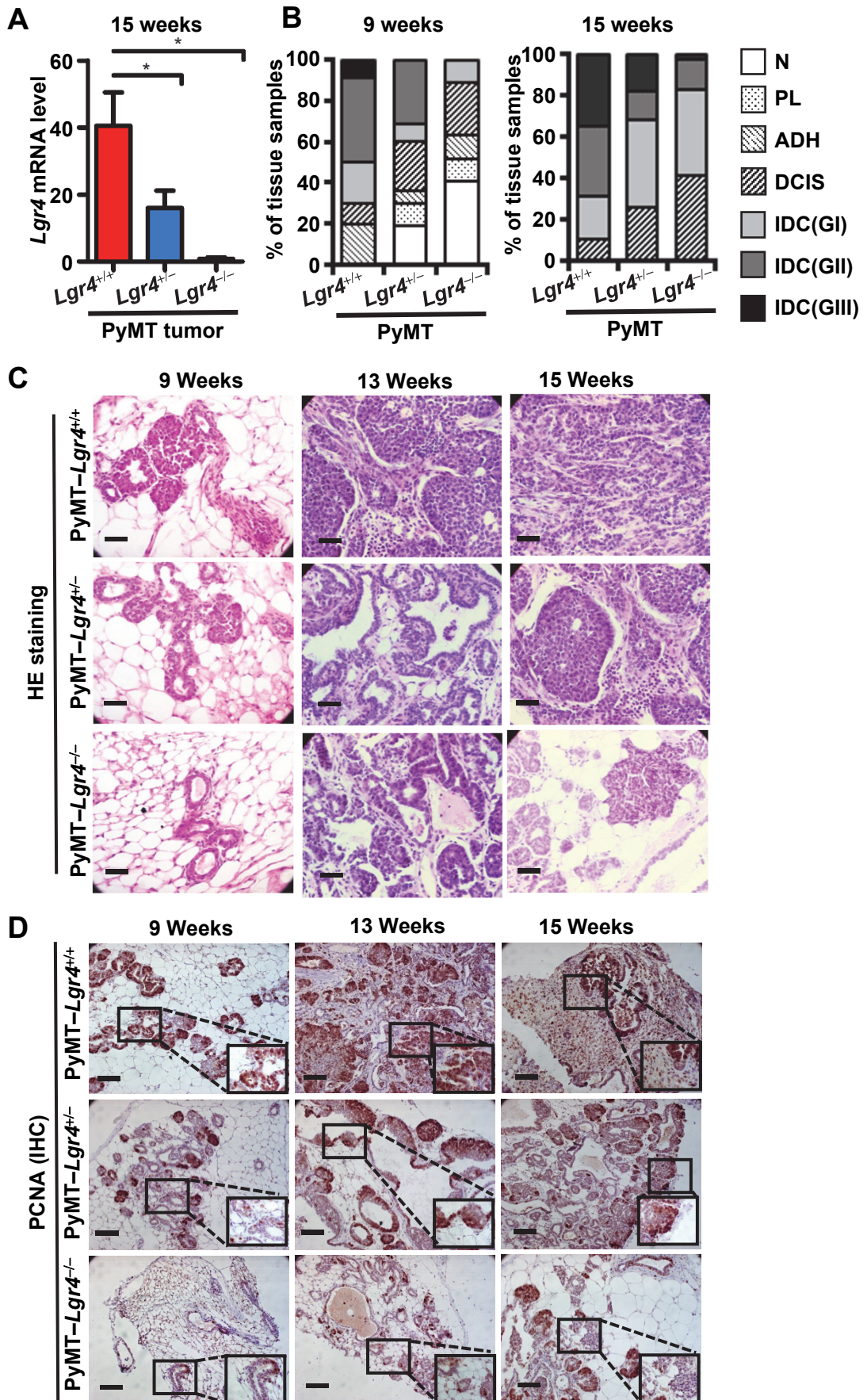




Figure S3





**Figure S4**

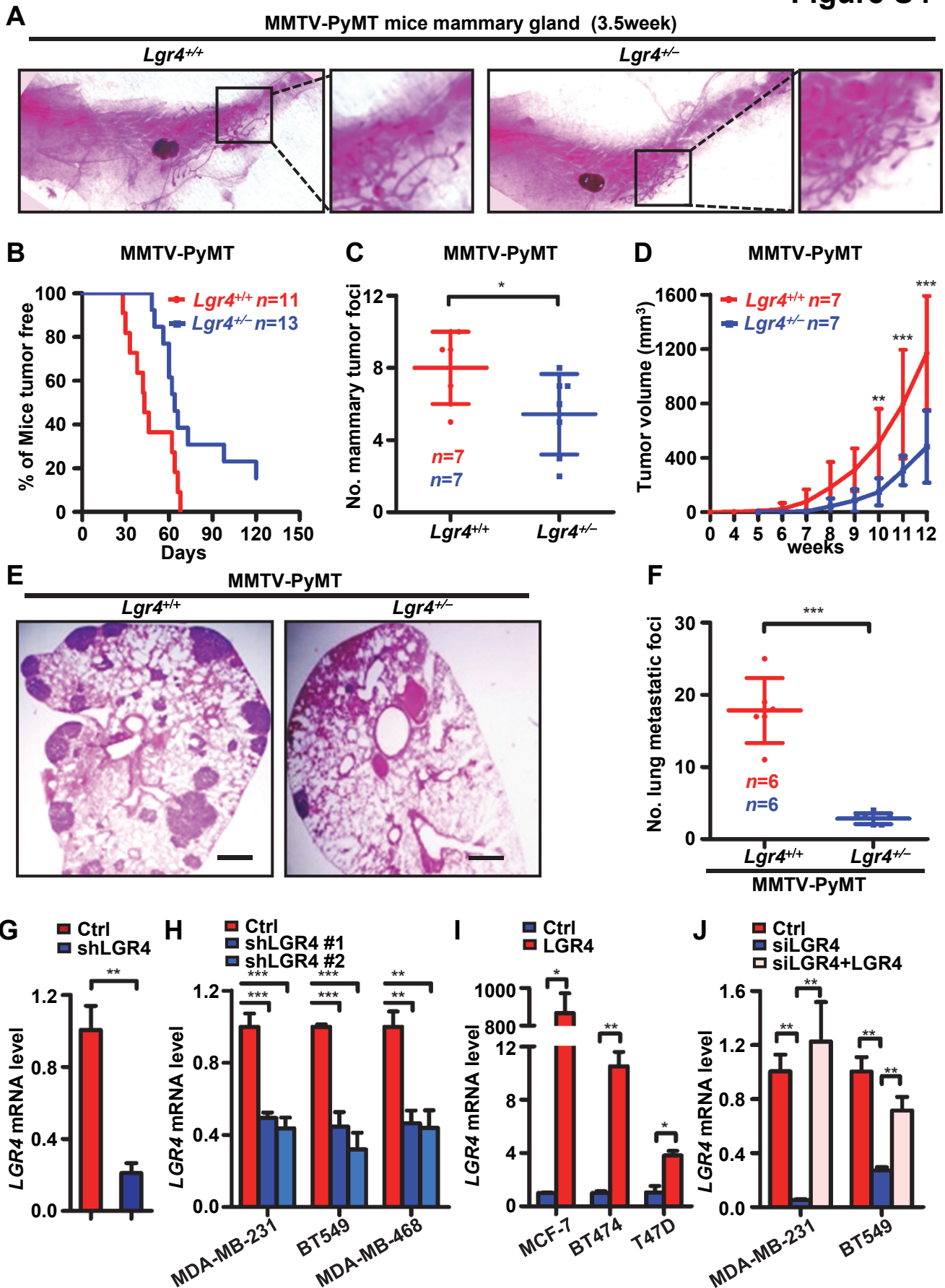


Figure S5

